Journal of Power Sources 190 (2009) 476–484

Contents lists available at ScienceDirect

Journal of Power Sources

journal homepage: www.elsevier.com/locate/jpowsour

A modeling study on the thermomechanical behavior of glass-ceramic and self-healing glass seals at elevated temperatures

N. Govindaraju [a], W.N. Liu [b], X. Sun [b], P. Singh [b], R.N. Singh [a,*]

[a] Department of Chemical and Materials Engineering, University of Cincinnati, Cincinnati, OH 45221, USA
[b] Pacific Northwest National Laboratory, Richland, WA 99354, USA

ARTICLE INFO

Article history:
Received 13 December 2008
Received in revised form 1 January 2009
Accepted 7 January 2009
Available online 19 January 2009

Keywords:
Solid Oxide Fuel Cell
Glass seals
Thermomechanical behavior
Modeling
Creep

ABSTRACT

Hermetic gas seals are critical components of planar Solid Oxide Fuel Cells (SOFCs). This article focuses on the comparative evaluation of a glass-ceramic seal developed by the Pacific Northwest National Laboratory (PNNL) and a self-healing glass seal developed by the University of Cincinnati. The stress and strain levels in the Positive electrode–Electrolyte–Negative electrode (PEN) seal in a single-cell stack are evaluated using a multi-physics simulation package developed at PNNL. Simulations were carried out with and without consideration of a clamping force and a stack body force, respectively. The results indicate that the overall stress and strain levels are dominated by the thermal expansion mismatches between the different cell components. Further, compared with the glass-ceramic, the self-healing glass results in a much lower steady state stress value due to its much lower stiffness at the operating temperature of the SOFC. It also exhibits much shorter relaxation times due to a high creep rate. It is also noted that the self-healing glass seal will experience continuing creep deformation at the operating temperature of a SOFC therefore resulting in possible overflow of the sealant material. Therefore, a stopper material may be required to maintain its geometric stability during operation.

1. Introduction

The volatility of the oil markets and the increasing concern with the environmental impact of noxious gas emissions have generated a renewed interest in the development of clean and efficient sources of power. In this context fuel cells are an attractive power source since energy conversion in a fuel cell is electrolytic thereby eliminating harmful gas emissions. Furthermore, it has been shown that fuel cells are more efficient at energy conversion as compared to the combustion of fossil fuels. Among various fuel cell technologies, Solid Oxide Fuel Cells (SOFCs) and Polymer Electrolyte Membrane Fuel Cells (PEMFCs) are the leading candidates under intensive research and development [1]. While PEMFCs are more suited for the automotive industry, SOFCs are the leading contenders for standalone power generation with a power generation range of 5–250 kW and lifetimes exceeding 40,000 h of operation [1]. The goal of SECA (Solid-state Energy Conversion Alliance), funded by the United States Department of Energy (DOE), is to develop commercial SOFC technology at the rate of $400/kW [2].

The successful development of such technology is however dependent on overcoming a series of technological hurdles. In contrast to PEMFCs, which operate at low temperature (<100 °C), the higher operating temperature of SOFCs poses significant technological challenges. Solid Oxide Fuel Cell design may be primarily categorized into two types viz., tubular and planar. Tubular SOFCs, by design, do not require a gas seal. Planar SOFCs offer a significant advantage of a compact design along with higher power densities, but require the incorporation of hermetic gas seals for efficient and effective channeling of fuel and oxygen. Seals are the most critical components in commercializing the planar SOFC technology—they must adequately prevent the leakage of air and fuel, effectively isolate the fuel from the oxidant, and be electrically insulating.

Mechanistically, there are two types of seals: compressive seals and rigid seals [3,4]. Compressive seals, as the name implies, involve the use of materials (such as metals or mica based composites) under compressive loads to ensure gas tight sealing as opposed to rigid seals which rely on effective bonding of the seal to the sealing surfaces. Therefore, in the case of rigid seals, physical properties such as the coefficient of thermal expansion (CTE) become critical since it is required that the CTE mismatch across the sealing interface be minimal. Rigid seals offer significant advantages over compressive seals which suffer from problems of oxide scaling and chemical stability under highly reactive environments in addition to the disadvantages of incorporating an externally applied load [3]. Among the rigid seals there are three separate approaches to sealing—glass seals, glass-ceramic seals and metal brazes. Among the glass seals, one area of significant interest is in the development of innovative self-healing glasses [3]. Self-healing glasses have

* Corresponding author. Tel.: +1 513 556 5172; fax: +1 513 556 3773.
E-mail address: Raj.Singh@uc.edu (R.N. Singh).

0378-7753/$ – see front matter © 2009 Elsevier B.V. All rights reserved.
doi:10.1016/j.jpowsour.2009.01.006

Nomenclature

A	area (m^2)
c	specific heat ($J\,kg^{-1}\,K^{-1}$)
C	concentration ($mol\,m^{-3}$)
E^0	Nernst potential (V)
E	Young's modulus (Pa)
F	Faraday constant ($C\,mol^{-1}$)
i	current density ($A\,m^{-2}$)
I	current (A)
l	length (m)
n	number of moles (mol)
p	partial pressure (Pa)
Q	volumetric heat flux ($W\,m^{-3}$)
r	reaction rate ($mol\,m^{-3}\,s^{-1}$)
R_G	universal gas constant ($J\,K^{-1}\,mol^{-1}$)
R	resistance (Ω)
t	time (s)
T	temperature (K)
u	volumetric flow rate ($m^3\,s^{-1}$)
V_v	voltage (V)
V	volume (m^3)
ε	strain
η	viscosity (Pa s)
λ	thermal conductivity ($W\,m^{-1}\,K$)
ρ	density ($kg\,m^{-3}$)
ρ_c	resistivity ($\Omega\,m$)
σ	stress (Pa)

the ability to effectively "repair" any cracks developed during thermal cycling when heated to a sufficiently high temperature. These sealant materials, if proven to meet the stringent long-term operating requirements, will offer a simple yet powerful solution to the problem of developing effective gas seals for SOFC applications.

As a step towards the realization of this goal, it is necessary to evaluate the mechanical performance of these seals in a fuel cell especially in relation to their interaction with other components present in the cell. Before conducting costly experimental trials, it is prudent and cost-effective to first evaluate the mechanical performance of self-healing glasses by simulating their interaction with other components present in a single-cell stack. The rationale behind carrying out a simulation study is to evaluate the performance of a component or several components in relation to each other. Apart from the apparent savings in cost and time, another significant benefit is the ability to "peer into" the system and study the effect of process parameters on parts which would be inaccessible experimentally. A methodical simulation study in conjunction with experiment is a very powerful tool which can shed valuable insights into the underlying complex physical phenomena and hence lead to a more reliable SOFC design with increased efficiency.

This article aims to quantify the viability of two different sealant materials by means of modeling their long-term performance in a single-cell stack. In order to provide a context for the work presented in this article a brief summary of recent relevant research is discussed below. It is to be noted here that the discussion presented below is by no means comprehensive, and the reader is encouraged to consult other sources [5–7] for a more complete overview of modeling studies carried out with respect to SOFCs.

Simulations of SOFC behavior may be broadly divided into two categories:

i. Microscopic Models
ii. Macroscopic Models

Microscopic modeling employs techniques such as Molecular Dynamics (MD) to investigate the transport phenomena in the atomic or nanoscale regime. These models, therefore, serve to enhance our understanding of the fundamental behavior of various materials in the SOFC stack and thereby help in the development of materials with tailored material properties.

Macroscopic models on the other hand ignore the microscopic details and instead employ macroscopic level constitutive equations to describe the coupling of heat, mass, electrochemical and momentum transport. Some macroscopic models in fact even simplify this approach further by treating the behavior of individual fuel cells as "black boxes" (thereby ignoring the performance of individual components in a single-cell) in order to carry out system level simulations [8,9]. Each of the above approaches serves to enhance understanding of SOFC behavior at different time and length scales and hence is important in its own right. The modeling work presented in this article is macroscopic in nature and involves, as mentioned earlier, the thermomechanical behavior of glass seals in a single-cell SOFC stack.

A large number of simulation studies have been carried out covering various aspects of the operation of Solid Oxide Fuel Cells and the different fundamental mechanisms governing the behavior of the fuel cells [5–7]. However, to date few models cover the complex multi-physics problem involving electrochemistry, fluid flow, heat transfer and their influence on the manifested mechanical behavior of a fuel cell. Yakabe et al. [10], performed studies to evaluate thermal stresses in an anode–electrolyte–cathode unit along with an interconnect layer. The modeling, based on the commercial STAR-CD software [11] from Computational Dynamics Ltd., involved coupled electrochemical, fluid flow, thermal and stress analysis. Selimovic et al. [12], utilized the FEMLAB software [13] from COMSOL AB to evaluate the thermal stresses in a two-dimensional model of a three layered structure (anode, electrolyte and cathode) with electrochemistry, in which thermal and flow calculations were performed by the finite volume method using FORTRAN. Laurencin et al. [14], modeled the coupled thermomechanical and electrochemical behavior in a circular three layer SOFC stack. Behavior of the sealant material was ignored in the aforementioned work. Müeller et al. [15], conducted an interesting study on the propagation of cracks in the presence of a sealant material, however the study focused only on the thermomechanical behavior and ignored fluid flow and electrochemical phenomena. Zhang et al. [16], used an analytical approach to calculate the residual stresses in a three layer anode–electrolyte–cathode stack, but the complicated nature of the calculations precluded the consideration of other factors influencing the functioning of an SOFC.

The very nature of the phenomena involved and their extremely complex interactions result in numerical simulations which are computationally intensive and therefore difficult to develop. There are only a few published studies to date which deal with thermomechanical behavior of SOFC seals in a "realistic" configuration viz., the modeling of the sealant materials in conjunction with other components in a fuel cell [17,18]. Lin et al. [17] conducted a detailed multi-physics study including fluid flow, heat transfer, electrochemistry and mechanical behavior using data available in published literature. Weil and Koeppel [18] presented recent results from finite element (FE) simulations of a planar cell using the foil-based seal, along with companion analyses of the more conventionally employed glass-ceramic and brazed joints. The behavior of self-healing glass seals was not considered in the aforementioned simulations. Furthermore, effects of creep in conjunction with the other transport phenomena on the evolution of stress and deformation of SOFC have not been considered so far [19]. In view of their critical role and given the high operating temperature of SOFCs with long designed lifetimes, it is imperative that more attention be paid to this aspect of the thermomechanical behavior of fuel cells as a

whole and glass seals in particular. The focus of this article is to provide a comparative evaluation of the time-dependent behavior of a glass-ceramic seal developed by the Pacific Northwest National Laboratory (PNNL) and a self-healing glass seal developed by the University of Cincinnati. The stress and strain levels in the PEN seal in a one cell stack are evaluated using a multi-physics simulation package developed at PNNL. Simulations were carried out with and without consideration of clamping force and body force, respectively. The results indicate that the overall stress and strain levels are dominated by the thermal expansion mismatches between the different cell components. Further, compared with the glass-ceramic seal, the self-healing glass seal results in a much lower steady state stress value due to its lower modulus at the operating temperature of the SOFC, and also exhibits much shorter relaxation times due to a high creep rate. It is to be noted that the self-healing glass seal will experience continuing creep deformation under the operating temperature of the SOFC, thus resulting in possible overflow of the sealing material under long-term operation. Therefore, a stopper material may need to be added to maintain its geometric stability during operation. This study will provide a quantitative basis for the development of an effective, stable sealant material.

2. Model formulation and simulation parameters

In order to model the behavior of the glass seals in a single-cell stack, a software module developed at PNNL, viz., SOFC-MP [20], was used. The software is based on the MSC.Marc® finite element program from MSC Software Corp., along with a proprietary module developed by PNNL for electrochemical (EC) as well as flow calculations. The EC module calculates the current distribution, gas species concentration and heat generation and uses the MSC.Marc® software to solve the heat transfer problem. The MSC.Marc® software is also used to calculate the time-dependent creep behavior of the stack using a user-defined material subroutine. The governing equations describing electrochemical, heat transfer, fluid flow and thermomechanical phenomena are given below along with a brief description of the underlying assumptions behind the equations—the reader is referred elsewhere [20–23] for a more in-depth discussion on these topics.

2.1. Electrochemistry

The EC module in SOFC-MP is capable of simulating electrochemical reactions with H_2 as the primary fuel as well as CO and composite fuels [20]. In the interest of brevity only the *I–V* relation involving H_2 as the fuel is given below, the equations for describing other fuel inputs may be found in [20,21].

$$V(i) = E^0 - iR_i - b\,\sinh^{-1}\left(\frac{i}{2i_0}\right) + \frac{R_G T}{4F}\,\ln\left(1-\frac{i}{i_{O_2}}\right) + \frac{R_G T}{2F}\,\ln\left(1-\frac{i}{i_{H_2}}\right) - \frac{R_G T}{2F}\,\ln\left(1+\frac{p^0_{H_2} i}{p^0_{H_2O} i_{H_2}}\right) \quad (1)$$

where E^0 is the Nernst potential, i is the current density, $b\sinh^{-1}(i/2i_0)$ is the activation polarization, R_G is the gas constant, T is the temperature, F the Faraday constant, i_{O_2} the oxygen transport limiting current, i_{H_2} the hydrogen transport limiting current, $p^0_{H_2O}$ and $p^0_{H_2}$ being the water and hydrogen partial pressures respectively. Finally, the resistance of the PEN structure, $R_i = R_p + R_e + R_n + R_b$, where R_p is the cathode resistance, R_e is the electrolyte resistance, R_n is the anode resistance and R_b is the bipolar resistance.

Eq. (1) is based on the following main assumptions [20,21]:

- The dominant mode of gas transport in the anode and the cathode is by binary diffusion through the pores in the electrode material. In other words, the effective binary diffusivity is obtained by multiplying the binary diffusion coefficient by the volume fraction of the porosity and by dividing it by the tortuosity factor.
- The electrodes have uniform microstructures through the thickness and the diffusion of the gas species is influenced by the porosity and tortuosity of the electrodes.
- The partial pressures of the gas species involved in the electrochemical reaction at the electrode–electrolyte interface are the same as the partial pressures outside the reaction zones.
- Temperature dependent resistances are employed for the anode, cathode and bipolar plate.

2.2. Fluid flow

The EC module simplifies the fluid flow problem by treating all fluid flow in the fuel cell as one-dimensional flow which is laminar in nature and by using simplified equations based on mass balance and flow rate to account for their behavior. This formulation circumvents the need to solve the complete fluid flow problem involving the Navier–Stokes equations and hence results in significant savings in computation time and resources. A simple mass balance detailed in Eq. (2) below is used to derive the rate of change of partial pressure of a particular species as a function of the current flow through the cell (I) and the gas flow rate (u) as shown in Eq. (3) for the case of hydrogen.

$$\frac{dn_k}{dt} = r_k\,dV_v - u\,dC_k \quad (2)$$

$$\frac{dp_{H_2}}{dt} = -\frac{IR_G T}{2Fu} \quad (3)$$

where n_k is the number of moles of species k, t is the time, r_k is the reaction rate per unit volume, V_v is the volume, u is the fluid velocity and C_k is the concentration of the species k, p_{H_2} is the hydrogen partial pressure. The coupling between the fluid flow and the electrochemical calculations is achieved through the current I in the above equation.

2.3. Heat transfer

As mentioned earlier, the MSC.Marc® software solves the heat transport problem (both steady state and transient) by the finite element method to provide the temperature distribution in the fuel cell stack [22]. The general form of the heat conduction equation in three-dimensions is given below.

$$\nabla\cdot(\lambda\nabla T) + Q = \rho c_p\frac{\partial T}{\partial t} \quad (4)$$

where λ is the thermal conductivity, Q is the volumetric heat flux, ρ the density, and c_p the specific heat.

The coupling between the EC module and the MSC.Marc® software is achieved through the volumetric heat generation term viz., Q. The heat generation in the fuel cell is calculated by assuming Joule heating due to the current flow I through the cell and the resistance $R(i)$ calculated from Eq. (1), i.e., from the calculated $V(i)$ as shown below.

$$Q = i^2\rho_c(i) = \frac{i^2R(i)A}{l} = \frac{i^2A}{l}\left(\frac{E^0 - V(i)}{i}\right) \quad (5)$$

The volumetric heat flux thus calculated is fed into the MSC.Marc® software via the user subroutine FLUX [23].

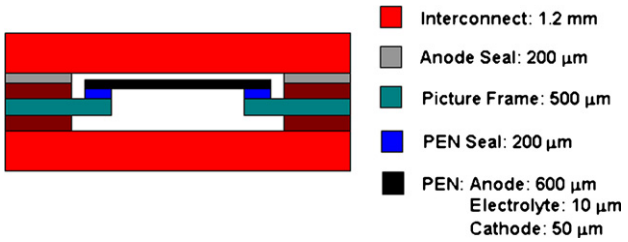

Fig. 1. Schematic diagram of the cross section of a Solid Oxide Fuel Cell—the thickness of the main components is given. Dimensions are not to scale.

Table 1
Material property values at room temperature (298 K) for the self-healing glass developed at the University of Cincinnati which were employed in the simulations.

Material property	Value
Young's modulus	70 GPa
Strength	70 MPa
Poisson's ratio	0.2
Viscosity	$\log(\eta) = 15.36(1000/T) - 5.46$ Pa s

2.4. Stack geometry and material properties

Fig. 1 shows a schematic cross section of the fuel cell model used along with the thickness of the main components. Except for the seals and the PEN structure, all the other materials are assumed to be SS-430. Snapshots of the individual components of a fuel cell unit are depicted in Fig. 2 below. Fig. 3 above illustrates the top view of the PEN seal along with its in-plane dimensions. Default geometric parameters in Mentat-FC are used for all the components of the single-cell stack.

Two different sealing materials were considered in this study:

i. Glass-ceramic: A $BaO–SiO_2$ system based glass-ceramic seal developed by PNNL and designated, with reference to a particular composition, as G18 [24].
ii. Self-healing glass: A silicate based self-healing glass developed at the University of Cincinnati was used for comparison with G18. Further details about the glass preparation and experimental evaluation of its physical properties may be found in [3].

The physical properties used in the simulations for the self-healing glass are given in Table 1. Since the Young's modulus data as a function of temperature was not available for the self-healing glass, the temperature dependent Young's modulus data for a pure amorphous glass [25] was used instead, under the assumption that their high temperature modulus may be similar since the room temperature modulus values for both the materials were the same. While we acknowledge that this assumption may not be entirely valid, it does provide a basis for a first order approximation to simulate the behavior of the seals until the relevant experimental data becomes available in the future. The temperature dependent moduli of pure amorphous glass and G18 after aging for 4 h are depicted in Fig. 4. It can be seen that the modulus of the aged glass-ceramic is nearly constant even at high temperature, and has a much higher

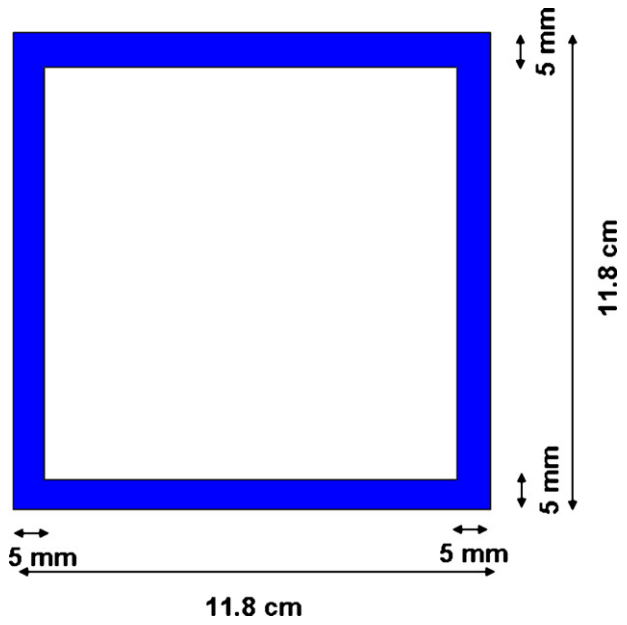

Fig. 3. Schematic diagram of the top view of the PEN seal. Dimensions are not to scale.

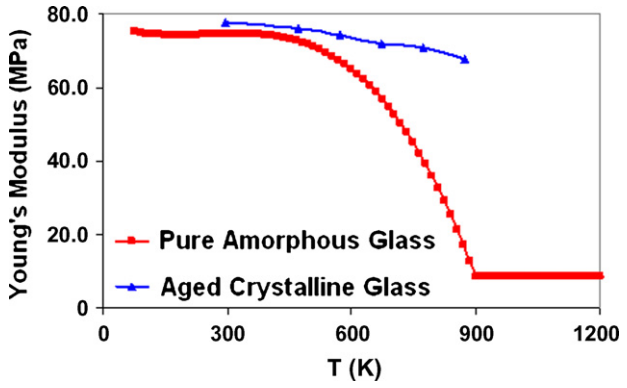

Fig. 4. Temperature dependent Young's moduli of pure amorphous and aged crystalline glasses.

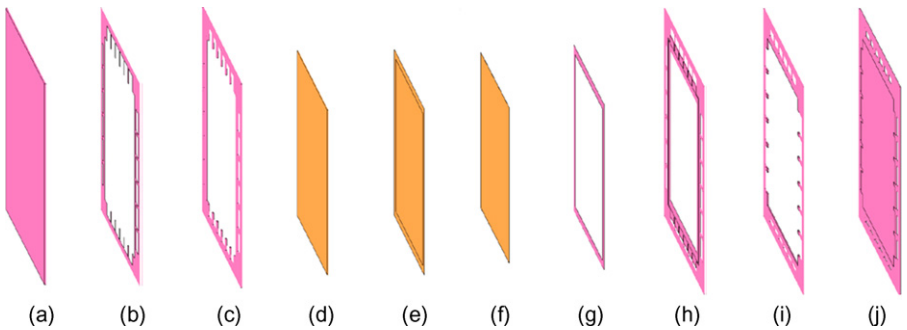

Fig. 2. Schematic diagram of the individual components in a single fuel cell unit: (a) Interconnect, (b) Anode Seal, (c) Fuel Frame, (d) Anode, (e) Electrolyte, (f) Cathode, (g) Anode Seal, (h) Air Frame, (i) Picture Frame and (j) Interconnect.

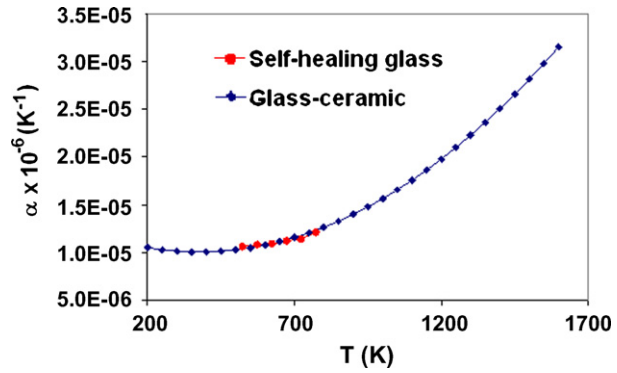

Fig. 5. Coefficient of thermal expansion (CTE) data used in the simulations.

value than the amorphous glass. The coefficients of thermal expansion (CTE) for both the sealing materials are plotted in Fig. 5.

2.5. Seal creep behaviors

Both the self-healing glass and the glass-ceramic sealants exhibit creep behavior at the operating temperature of the SOFC. The experimentally determined creep curves for the self-healing glass and the aged glass-ceramic are depicted in Fig. 6.

The creep behavior of the self-healing glass sealant is modeled by Eq. (6):

$$\dot{\varepsilon}_{\text{eff}} = A\frac{\sigma_0}{3\eta(T)} \tag{6}$$

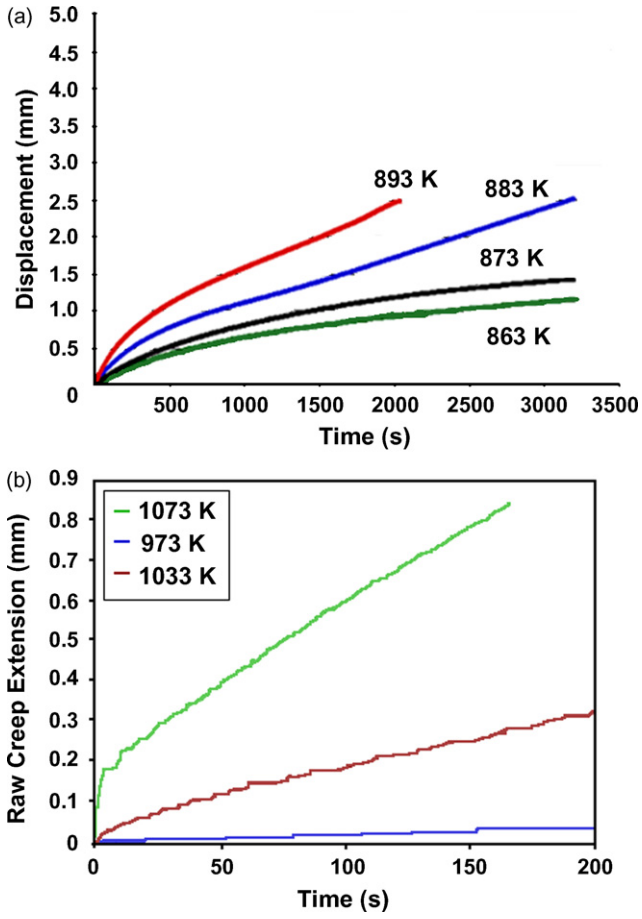

Fig. 6. Experimental creep behavior for (a) the self-healing glass and (b) aged glass-ceramic at different temperatures.

Table 2
Comparison of experimental creep strain rates for self-healing glass and glass-ceramic under uniaxial stress of 30 MPa at 1000 K.

	Self-healing glass	Glass-ceramic
Creep strain rate (at 1000 K)	1.0e−3 s^{-1}	1.0e−6 s^{-1}

where A is a constant and $\eta(T)$ is the temperature dependent viscosity, which is determined from the creep test results at different temperatures as shown in Fig. 6(a).

To capture the creep behavior of the glass-ceramic sealant, a two phase standard viscoelastic solid model was adopted. For the glassy phase, the strain included two components, i.e., elastic and viscous strains, respectively, as

$$\varepsilon_{gl} = \varepsilon^{v}_{gl} + \varepsilon^{e}_{gl} \tag{7}$$

where

$$\varepsilon^{e}_{gl} = \frac{\sigma_{gl}}{E_{gl}(T)} \tag{8}$$

$$\dot{\varepsilon}^{v}_{gl} = \frac{\sigma_{gl}}{\eta_{gl}(T)} \tag{9}$$

the temperature dependent viscosity $\eta_{gl}(T)$ is determined from the creep test results at different temperatures as shown in Fig. 6(b).

In general, the ceramic phase is considered to undergo elastic deformation only, therefore, its stress and strain relationship will follow Hooke's law:

$$\varepsilon_c = \frac{\sigma_c}{E_c(T)} \tag{10}$$

The overall stress and strain relationship is governed by

$$\sigma = \sigma_{gl} + \sigma_c \tag{11}$$

$$\varepsilon = \varepsilon_{gl} = \varepsilon_c \tag{12}$$

The above two creep models are incorporated into the MSC.Marc® software via the user-defined subroutine CRPLAW [23].

For reference, Table 2 lists the experimental creep strain rate of both the self-healing glass and glass-ceramic at 1000 K under uniaxial stress of 30 MPa. It can be seen that the creep rate of the self-healing glass is about 1000 times higher than that of the glass-ceramic.

3. Results and discussion

In order to evaluate the creep behavior of the two different seal materials, time-dependent creep simulations were carried out using the steady state operating temperature profile, which was calculated by SOFC-MP using the stack geometry and material properties described above. The initial stress-free temperature was 1073 K (800 °C), which was the stack assembly temperature. The goal was to quantitatively compare the time-dependent behavior of the two sealant materials by considering the interactions of the different stack components present in the SOFC during steady state operation.

A series of simulations were carried out with and without the consideration of body force and stack clamping force, and the results will be discussed later in this section. Note that all the results discussed below refer exclusively to the PEN seal. The rationale behind the incremental approach was to evaluate the effect of fundamental physical properties (Young's modulus, CTE) on the overall stress distributions in the absence of a body force, following which the addition of this force along with an externally applied clamping force would lead to an elucidation of the effect of the different parameters on the stress distributions in the PEN seal.

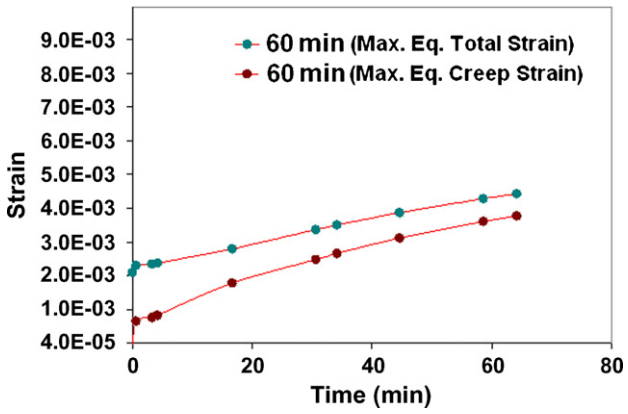

Fig. 7. Maximum equivalent total strain and maximum equivalent creep strain as a function of the hold time for the PEN seal with self-healing glass, at the operating temperature.

3.1. Without body force (gravity) and clamping force

Due to the high creep rate of the self-healing glass, very small time increments had to be used in the simulation of long-term behavior of these sealant materials. Therefore, initially, the effect of hold times at the operating temperature profile on the long-term behavior of the PEN seals (in the case of the self-healing glass) was studied with the aim of deciding on a realistic holding time thereby resulting in significant savings in computing time. Three holding times were chosen for this purpose—0.07 h (4.2 min), 0.5 h and 1 h. Fig. 7 shows the maximum equivalent total strain and the maximum equivalent creep strain for a hold time of 1 h. It is to be noted here that the curves for lower holding times, i.e., 0.07 h and 0.5 h are identical and are not reproduced. It can be seen that after the initial steep increase of these strains, caused by the temperature drop from the stress-free temperature to the operating temperature profile of a single-cell stack, maximum equivalent total strain and the maximum equivalent creep strain continued to increase, and the rate of increase tapered off slightly with time within 1 h. The maximum equivalent von Mises stress values, for the same hold times, are presented in Fig. 8. It can be noted that the von Mises stress falls from a maximum value of about 4 MPa to around 40 kPa within a time span of about 10 min. A similar trend is observed in the σ_{33} (normal stress through the thickness of the seal) and σ_{11} (normal stress in the seal plane) plots with respect to time (Fig. 8). Therefore, the stresses in the seal reached their asymptotic values after a

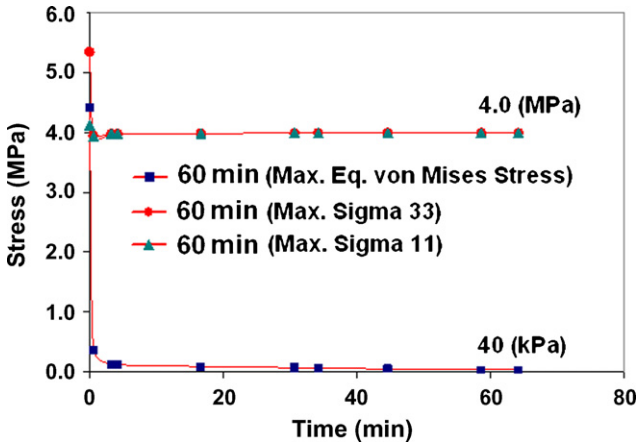

Fig. 8. Maximum equivalent von Mises stress, maximum σ_{33} component of stress and maximum σ_{11} component of stress for the PEN seal with self-healing glass as a function of hold time, at the operating temperature.

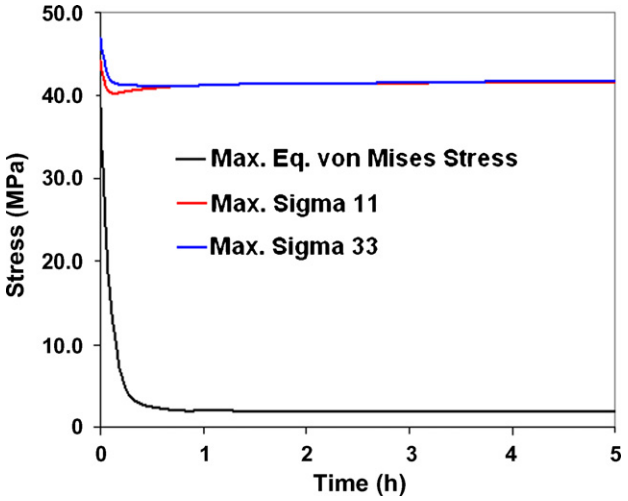

Fig. 9. Stress history for the PEN seal with the glass-ceramic as the seal material.

1 h relaxation time. From the stress relaxation point of view, therefore, a holding time of 1 h was chosen for further simulations of self-healing glass seals.

Fig. 9 shows the stress history, i.e., maximum equivalent von Mises stress, maximum σ_{11}, and σ_{33}, for the PEN seal with the glass-ceramic. The maximum equivalent total strain and maximum equivalent creep strain are depicted in Fig. 10 over the creep time. The results are similar to those obtained with the self-healing amorphous glass, wherein the von Mises stress is released rapidly, the normal stresses σ_{11} and σ_{33} are constant after a small drop, because the hydrostatic pressure could not be relaxed by creep deformation. Compared with the self-healing amorphous glass, the time to relax the shear/deviation stress is much longer—close to 1 h in the case of the glass-ceramic while in the case of the self-healing glass the time scales are of the order of few minutes. Also, the value of the maximum equivalent von Mises stress in the case of the glass-ceramic after stress relaxation is of the order of 1 MPa as opposed to 40 kPa in the case of the self-healing glass. This is because the glass-ceramic seal material possesses high modulus at the operating temperature of the SOFC due to the presence of the ceramic phase, but the modulus of the amorphous self-healing glass at the high operating temperature of SOFC is only about 1/10 of its room temperature value. In addition, it may be noted that the maximum

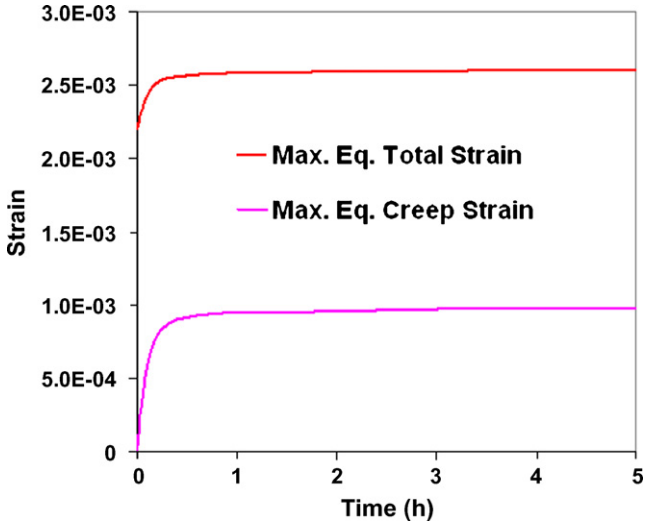

Fig. 10. Equivalent strain history in the PEN seal with the glass-ceramic as the seal material.

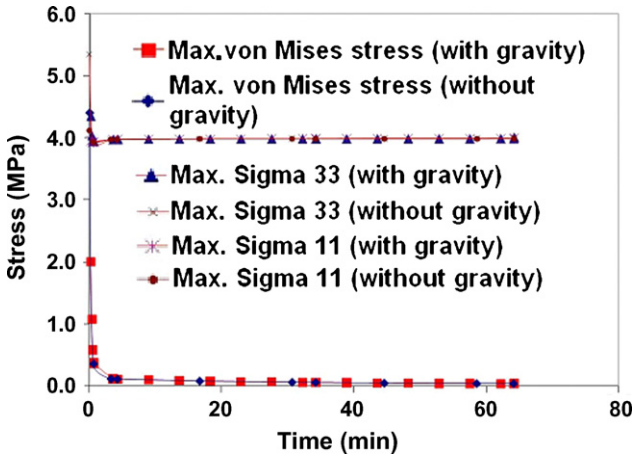

Fig. 11. Maximum equivalent von Mises stress, maximum σ_{33} and maximum σ_{11} with and without the presence of gravity in the PEN seal with self-healing glass at the operating temperature.

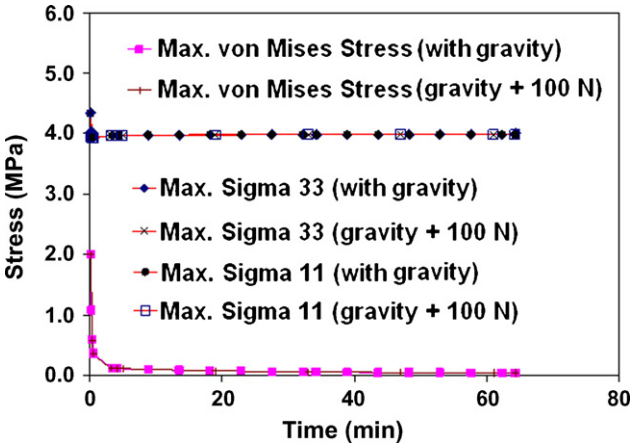

Fig. 13. Maximum equivalent von Mises stress, maximum σ_{11} and maximum σ_{33} under different loading conditions in the PEN seal with self-healing glass at the operating temperature.

equivalent total strain and creep strain are constant after the initial creep stage, i.e., no overflow of the glass-ceramic seal material will occur during the operation of the SOFC stack.

3.2. Effect of gravity

Using the 1 h hold time, the next step was to evaluate the effect of gravity on the stresses in PEN seals and compare them to the results without consideration of gravity presented in the previous section, as shown in Figs. 11 and 12. In the interest of brevity only the plots for the stress are presented here since the plots for the strains are identical to Figs. 7 and 10. It can be seen that the maximum equivalent von Mises stress, the components σ_{33} and σ_{11} are essentially unchanged by the presence of gravity, i.e., body force. These results indicate that the most significant contribution to the stresses in the PEN seal is the CTE mismatch between different components in the SOFC stack.

3.3. Effect of gravity and applied clamping load

Next, the effects of the stack clamping force on the stresses in the PEN seal were numerically evaluated. Point loads were applied to the top and bottom interconnects at the center points of the four corners to simulate the force due to clamping bolts. Two different loading conditions were considered—a total load of 10 N and 100 N for the case of the self-healing glass and a 100 N load for the glass-ceramic. These load levels were chosen such that the effects of an order magnitude change in the applied load could be evaluated. The stress levels in the two seals as a function of time are presented in Figs. 13 and 14 for both the sealant materials. It should be noted here that the results for the 10 N applied load (in the case of the self-healing glass seal) are identical to that of the 100 N load and are not reproduced here. Also, the strain distributions for both the sealant materials are identical to those presented in Figs. 7 and 10.

It is evident from these results that there is no significant difference in the stress and strain distributions even in the presence of an externally applied stack clamping load for both sealant materials. For illustration, Fig. 15 shows the von Mises stress contour bands for the PEN seal with no body force or external loads considered for the self-healing glass material.

From the above discussions, it may be concluded that the most significant contributors to the stress variations in the PEN seal are the physical property differences (primarily Young's modulus and CTE) between the different materials used in the fuel cell. The significant differences in the behavior of the two materials are illustrated by Fig. 16. Fig. 16(a) is a comparative plot of the strain levels in the

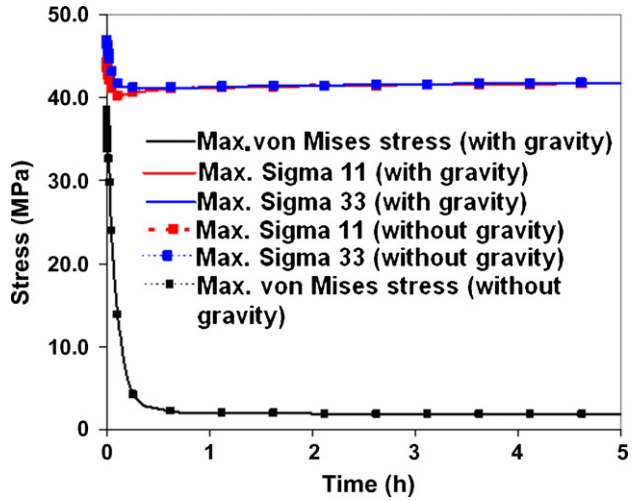

Fig. 12. Effect of gravity on the stresses in the PEN seal with glass-ceramic at the operating temperature.

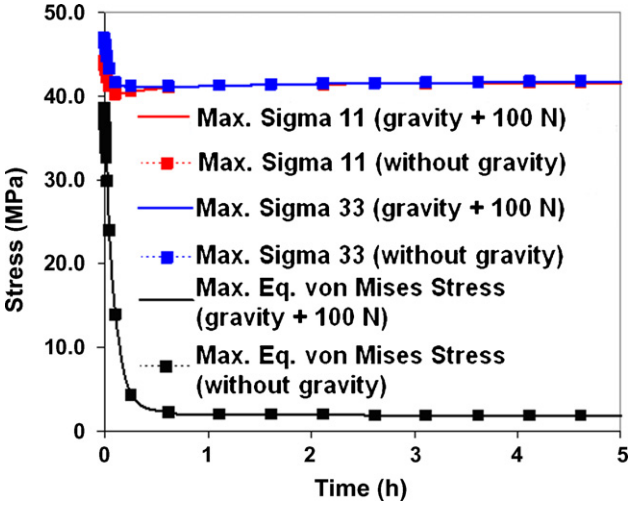

Fig. 14. Stress history for the PEN seal with glass-ceramic at the operating temperature under different loading conditions.

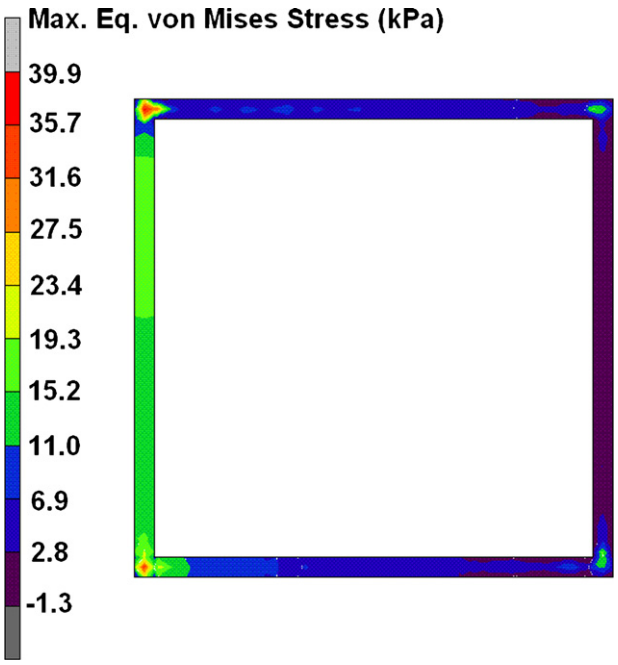

Fig. 15. Contour band plot of the equivalent von Mises stress in the PEN seal with self-healing glass in the absence of gravity and an externally applied load.

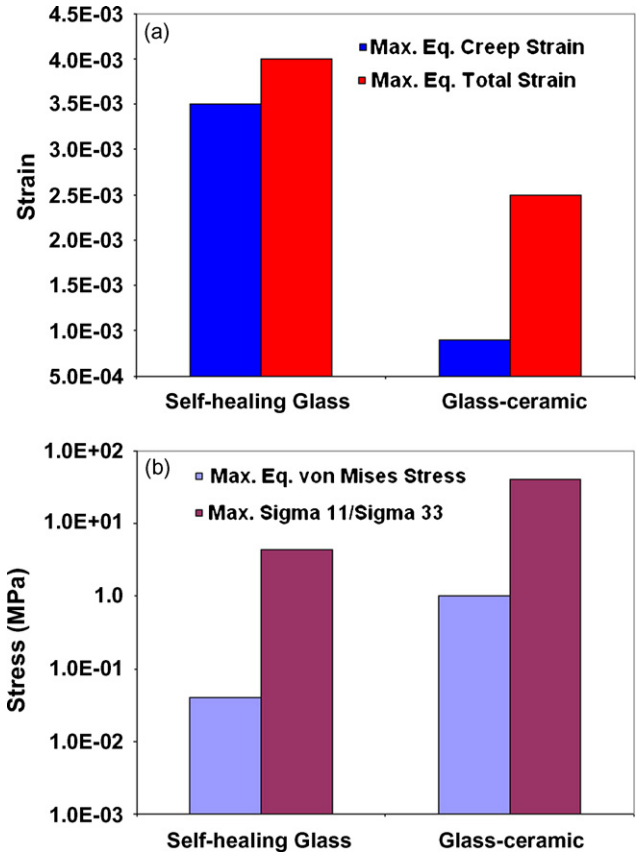

Fig. 16. Comparative plots of (a) strain and (b) stress levels in the glass-ceramic and self-healing glass seals at the operating temperature. The plots show significant differences in the values for both stress and strain in these materials after 1 h of operation.

two sealant materials after 1 h of operation. It can be seen from this plot that while the strain values for both the materials are within the same order of magnitude, the self-healing glass exhibits higher strain values as compared to the glass-ceramic material. Also, it should be noted that the total strain for the glass-ceramic seal reaches an asymptotic value after 1 h of operation, but the total strain for the self-healing glass seal keeps increasing after 1 h of operation (c.f., Figs. 7 and 10). Fig. 16(b) is a comparative plot of the stress levels in the two sealant materials after 1 h of operation. It can be seen that there is at least an order of magnitude difference in the stress values with the self-healing glass displaying lower stress values. Also, stress relaxation is achieved during the first several minutes of steady state operation for the self-healing glass seal. For the glass-ceramic seal, it takes about an hour. These results indicate the advantages of the self-healing glass seal in managing the operating stress levels in the seal. They also indicate that a potential area for further development for this sealing material lie in controlling its total creep deformation during the desired operating duration of an SOFC.

4. Conclusions

In this paper, stack level simulation studies were carried out to evaluate the time-dependent stress and strain behaviors in the PEN seal fabricated using a glass-ceramic and a self-healing glass. The simulations utilize coupled electrochemical, fluid flow, heat transfer and thermomechanical analyses. The results indicate that for both the materials the dominant effects on the resultant stresses and strains at the operating temperature of the SOFC are due to mismatch of CTE of the different stack components. Further, it is found that the stresses at the operating temperature in the case of the self-healing glass are significantly lower as compared to the glass-ceramic seal, due to its much lower modulus at the operating temperature of SOFC. The self-healing glass sealant also exhibits much shorter relaxation times due to its high creep rate, thereby indicating that the self-healing glass has the potential to be a simple yet effective sealing material from a seal stress management perspective. However, it is to be noted that the self-healing glass seal will experience continuing creep deformation under the operating temperature of the SOFC therefore resulting in possible overflow of the sealing material. Therefore, a stopper material may need to be added to maintain its geometric stability during operation. Simulation studies can help accelerate the material development process by screening the effects of different stopper material designs and their implementation. Further simulation studies are also planned to evaluate the effects of thermal cycling, residual stresses and various other load combinations on the thermomechanical behavior of different seal materials to holistically examine the time-dependent seal integrity and reliability under long-term operation.

Acknowledgements

The Pacific Northwest National Laboratory is operated by Battelle Memorial Institute for the United States Department of Energy under Contract DE-AC06-76RL01830. The work summarized in this report was funded as part of the Solid-State Energy Conversion Alliance (SECA) Core Technology Program by the U.S. Department of Energy's National Energy Technology Laboratory (NETL). The University of Cincinnati authors gratefully acknowledge the support for this work under the SECA program DOE contract DE-FC2604NT42227, the University of Cincinnati, and the stewardship of Dr. A. Manivannan. The authors would also like to acknowledge the help and technical discussions with Dr. Brian Koeppel.

References

[1] R.W. Lashway, MRS Bulletin 30 (2005) 581–583.
[2] http://www.netl.doe.gov/technologies/coalpower/fuelcells/seca/.
[3] R.N. Singh, International Journal of Applied Ceramic Technology 4 (2) (2007) 134–144.
[4] J.W. Fergus, Journal of Power Sources 147 (2005) 46–47.
[5] S. Kakaç, A. Pramuanjaroenkij, X.Y. Zhou, International Journal of Hydrogen Energy 32 (2007) 761–786.
[6] V.M. Janardhanan, O. Deutschmann, Zeitschrift für Physikalische Chemie 221 (2007) 443–479.
[7] R. Bove, S. Ubertini, Journal of Power Sources 159 (2006) 543–559.
[8] L. Petruzzi, S. Cocchi, F. Fineschi, Journal of Power Sources 118 (2003) 96–107.
[9] N. Lu, Q. Li, X. Sun, M.A. Khaleel, Journal of Power Sources 161 (2006) 938–948.
[10] H. Yakabe, T. Ogirawa, H. Hishinuma, I. Yasuda, Journal of Power Sources 102 (2001) 144–154.
[11] http://www.cd-adapco.com/products/STAR-CD/index.html.
[12] A. Selimovic, M. Kemm, T. Torisson, M. Assadi, Journal of Power Sources 145 (2005) 463–469.
[13] http://www.comsol.com/.
[14] J. Laurencin, B. Morel, Y. Bultel, F. Lefebvre-Joud, Fuel Cells 6 (1) (2006) 64–70.
[15] A. Müeller, S. Goswami, W. Becker, D. Stolten, L.G.J. de Haart, R.W. Steinbrech, Fuel Cells 6 (2) (2006) 107–112.
[16] T. Zhang, Q. Zhu, W.L. Huang, Z. Xie, X. Xin, Journal of Power Sources 182 (2008) 540–545.
[17] C.-K. Lin, T.-T. Chen, Y.-P. Chyou, L.-K. Chiang, Journal of Power Sources 164 (2007) 238–251.
[18] K.S. Weil, B.J. Koeppel, Journal of Power Sources 180 (2008) 343–353.
[19] W.N. Liu, X. Sun, M. Khaleel, Effects of Interconnect creep on long-term performance of one-cell stacks of SOFC, in: Proceedings of the 32nd International Conference & Exposition on Advanced Ceramics & Composites proceedings, Daytona Beach, FL, USA, January 28–February 1, 2008.
[20] M.A. Khaleel, Z. Lin, P. Singh, W. Surdoval, D. Collin, Journal of Power Sources 130 (2004) 136–148.
[21] J.-W. Kim, A.V. Virkar, K.-Z. Fung, K. Mehta, S.C. Singhal, Journal of the Electrochemical Society 146 (1) (1999) 69–78.
[22] MSC, Marc® Software Manual Volume A: Theory and User Information (Version 2005), MSC Software Corporation, Santa Ana, CA, USA, 2004.
[23] MSC, Marc® Software Manual Volume D: User Subroutines and Special Routines (Version 2005), MSC Software Corporation, Santa Ana, CA, USA, 2004.
[24] K.S. Weil, J.E. Deibler, J.S. Hardy, D.S. Kim, G.G. Xia, L.A. Chick, C.A. Coyle, Journal of Materials Engineering and Performance 13 (3) (2004) 316–326.
[25] D.A. McGraw, Journal of the American Ceramic Society 35 (1) (1952) 22–27.